This is the accepted manuscript made available via CHORUS. The article has been published as:

Evidence of lattice deformation induced metal-insulator transition in math xmlns="http://www.w3.org/1998/Math/MathML">mrow>msub>mi>Ti/mi>mn>2/mn>/msub>msub>mi mathvariant="normal">O/mi>mn>3/mn>/msub>/mrow>/math>

K. Yoshimatsu, S. Miyazaki, N. Hasegawa, and H. Kumigashira

Phys. Rev. B **106**, L081110 — Published 10 August 2022

DOI: 10.1103/PhysRevB.106.L081110

Evidence of lattice deformation induced metal-insulator transition in Ti_2O_3

K. Yoshimatsu[1,2*], S. Miyazaki[1], N. Hasegawa[1], and H. Kumigashira[1,2]

[1]*Institute of Multidisciplinary Research for Advanced Materials, Tohoku University, Sendai, Miyagi 980-8577, Japan*

[2]*Materials Research Center for Element Strategy (MCES), Tokyo Institute of Technology, Yokohama 226-8503, Japan*

Received date:

*Author to whom correspondence should be addressed; E-mail: kohei.yoshimatsu.c6@tohoku.ac.jp

Abstract

We synthesized Ti_2O_3 epitaxial films with continuously varying ratios of the *c*-axis to *a*-axis lattice constants (*c*/*a* ratios) on 4H-SiC (0001) substrates and investigated their structural and electronic properties. Ti_2O_3 films with a wide range of *c*/*a* ratios were fabricated in a controllable fashion by changing the growth temperature. As the *c*/*a* ratio at room temperature increased, the metal-insulator transition (MIT) temperature systematically decreased and eventually the MIT disappeared. Detailed analyses revealed that the MIT occurred at a critical *c*/*a* ratio of 2.68. The critical *c*/*a* ratio for the occurrence of the MIT was also reproduced by density functional theory calculations. These results provide evidence for the origin of the MIT in Ti_2O_3. The MIT is not a Mott transition induced by temperature, but a gradual semimetal-to-semiconductor transition induced by lattice deformation.

INTRODUCTION

Corundum-type titanium sesquioxide (Ti_2O_3) is a well-known $3d^1$ transition-metal oxide, and it exhibits a peculiar metal-insulator transition (MIT) [1]. Ti_2O_3 is a narrow-gap semiconductor with a gap of approximately 100 meV at room temperature (RT) and shows a transition to semimetallic states at a temperature of approximately 450 K that can occur over a broad temperature range of approximately 150 K [1–10]. The MIT is characterized by a concomitant drastic modification of the ratio of the *c*-axis to *a*-axis lattice constants (*c*/*a* ratio) in the crystal, without changing the crystal symmetry [5–8]. The MIT is unique to Ti_2O_3 among most other transition-metal oxide systems; thus, the MIT mechanism is discussed as one of the longstanding issues in condensed matter physics [1–15].

The most relevant mechanism of the MIT is the overlap of the a_{1g} and e_g^{π} bands due to the modulation of the c/*a* ratio (i.e., the Ti–Ti distance along the *c*-axis). In trigonally distorted TiO_6 octahedra, the t_{2g} levels split into a_{1g} and e_g^{π} levels. The a_{1g} orbitals between the face-sharing TiO_6 octahedra along the *c*-axis are strongly hybridized, thereby forming the a_{1g} and a_{1g}* bands. The e_g^{π} orbitals that expand in the

46 *a*–*b* plane are less hybridized, thereby forming e_g^{π} + e_g^{π}* bands, which lie between the
47 a_{1g} and a_{1g}* bands. When the Ti–Ti distance along the *c*-axis is short, the e_g^{π} + e_g^{π}*
48 bands do not overlap with the a_{1g} bands [6, 7]. Accordingly, all Ti 3*d* electrons
49 completely occupy the a_{1g} bands; consequently, a narrow gap is formed at the Fermi
50 level (E_F) [3]. Although the above phenomenological model can qualitatively explain
51 the MIT mechanism, band-structure calculations indicated the importance of electron
52 correlation in the MIT of Ti_2O_3 [11, 16]. Thus, the origin of the MIT remains under
53 debate.

54 The most straightforward approach to address the origin of the MIT is to
55 investigate the relationship between the MIT and *c*/*a* ratio. Epitaxial thin films provide
56 one of the best systems for such analyses, because they offer high flexibility to
57 accommodate various crystal-lattice structures. Indeed, epitaxial Ti_2O_3 films with two
58 different *c*/*a* ratios were successfully synthesized on α-Al_2O_3 (0001) substrates at two
59 different growth temperatures (T_g) [14]. Although a significant lattice mismatch (8.3%)
60 prevented coherent growth of the films [13, 14, 17–19], Ti_2O_3 films grown at high T_g
61 had a slightly larger *c*/*a* ratio and lower MIT temperature (T_{MIT}) than those of the bulk

material. The other Ti_2O_3 films grown at low T_g had a considerably large c/a ratio and metallic conductivity over the entire measured temperature range [14]. Unfortunately, owing to the formation of a secondary phase in Ti_2O_3 films grown on α-Al_2O_3 (0001) substrates in a certain temperature range, the systematic control of the structural and electronic properties by changing T_g has not yet been demonstrated [14, 17, 20]. In particular, there is no information on how T_{MIT} changes as a function of the c/a ratio, which has hindered the understanding of this material.

In this study, we synthesized Ti_2O_3 films with systematically varying c/a ratios on 4H-SiC (0001) substrates [21]. Owing to the similarity in the local structures of Ti_2O_3 and 4H-SiC on the (0001) planes [22] (see Fig. S1 in Supplemental Material [23]), the corundum-type Ti_2O_3 phase was stabilized over a wide T_g range of 500–1050℃. In the obtained Ti_2O_3 films, the c/a ratio at RT (c_{RT}/a_{RT}) was controllable from 2.672 to 2.821 by changing T_g. As c_{RT}/a_{RT} increased, T_{MIT} systematically decreased, and finally, MIT disappeared at all measurement temperatures. By considering the thermal lattice expansion of Ti_2O_3, we revealed that the MIT occurred at a critical c/a ratio of 2.68 in both bulk and films. The critical c/a ratio was also reproduced using

78 calculations based on density functional theory (DFT). These results indicate that the
79 MIT is not a Mott transition induced by temperature, but a gradual
80 semimetal-to-semiconductor transition induced by lattice deformation in Ti_2O_3.
81
82 **EXPERIMENTAL SECTION**
83 Ti_2O_3 films were grown on 4H-SiC (0001) substrates using pulsed-laser
84 deposition (PLD) [13, 14, 17, 19, 20, 24]. A polycrystalline TiO ceramic tablet (3N
85 purity, Toshima Co., Ltd.) was used as the PLD target. A Nd:$Y_3Al_5O_{12}$ laser with
86 fourth-harmonic generation (λ = 266 nm) was used to ablate the target. The laser
87 frequency and fluence were set to 10 Hz and approximately 0.5 J/cm^2, respectively,
88 where the deposition rate of the Ti_2O_3 films was set to approximately 100 nm/h. The
89 film thickness was fixed at approximately 100 nm, as confirmed using a stylus-type
90 profiler. A constant substrate temperature was set in the range of 500–1050℃. Oxygen
91 gas (6N purity) was fed into the PLD chamber to maintain an oxygen partial pressure of
92 5.0×10^{-7} Torr. The supply of O_2 gas was immediately stopped after deposition, and the

substrate was quenched. Both procedures prevent additional oxidation during the cooling of Ti_2O_3 films [13–15, 20, 25].

The crystal structures of the films were characterized by Raman spectroscopy and X-ray diffraction (XRD). XRD measurements were performed at RT using a Rigaku SmartLab 9 kW diffractometer with Cu Kα1 radiation. The formation of corundum-type Ti_2O_3 films was confirmed using Raman spectroscopy [24, 26–32] (see Fig. S2 in Supplemental Material [23]). The out-of-plane (0001) orientation of the Ti_2O_3 films was revealed by out-of-plane XRD measurements (see Fig. S3 in Supplemental Material [23]). The temperature dependence of the resistivity was measured in a standard four-terminal geometry over the temperature range of 20 to 650 K.

DFT calculations were performed using Quantum ESPRESSO simulation software [33, 34]. A rhombohedral primitive cell was chosen for the calculations to reduce computational cost. Ultrasoft pseudopotentials were used, wherein Ti 3*s*, 3*p*, 3*d*, and 4*s* and O 2*s* and 2*p* atomic levels were included as valence-band states. The Perdew–Burke–Ernzerhof generalized gradient approximation (PBE-GGA) functional was used for the exchange–correlation potentials [35]. The kinetic energy and

charge-density cut-offs were set to 60 and 600 Ry, respectively. The Ti and O positions were optimized by a structural relaxation routine implementing the Monkhorst–Pack scheme with a 6 × 6 × 6 k-mesh in self-consistent calculations [36]. Accuracy of the total energy was less than 10^{-10} Ry at the end of the self-consistent calculations. The density of states (DOS) of the valence-band states was integrated using the tetrahedron method within a denser 12 × 12 × 12 k-mesh in non-self-consistent calculations [37]. The details of the DFT calculations were described elsewhere [14,15].

RESULTS & DISCUSSION

Figure 1 shows reciprocal space maps (RSMs) of the Ti_2O_3 films grown at various T_g values, demonstrating that the lattice constants of the Ti_2O_3 films were controllable by varying T_g. The 4H-SiC 10–19 and Ti_2O_3 11–2$\underline{12}$ reciprocal points were simultaneously observed in the RSMs. The Ti_2O_3 11–2$\underline{12}$ reciprocal points gradually shifted toward the small Q_z (large Q_x) direction with decreasing T_g, indicating elongation of *c* (shortening of *a*) in the films.

The a and c values of the Ti_2O_3 films obtained from the RSMs are summarized in Fig. 2(a). As shown in Fig. 2(a), c increased monotonically from 13.66 to 14.03 Å as T_g decreased from 1050 to 500°C. In contrast, a showed the opposite trend to that of c; a decreased monotonically as T_g decreased. The a values were 5.102 and 4.986 Å for films grown at 1050 and 500°C, respectively. In comparison to bulk Ti_2O_3, the Ti_2O_3 films had larger c and smaller a, regardless of T_g. Note that the trends in the lattice deformations by changing T_g are consistent with those of a previous report, wherein the Ti_2O_3 films were grown on α-Al_2O_3 (0001) substrates [14].

The resulting c_{RT}/a_{RT} ratios are plotted in Fig. 2(b) as a function of T_g. As expected from Fig. 2(a), the c_{RT}/a_{RT} ratio increased monotonically with decreasing T_g, suggesting linear controllability of the c/a ratio in the Ti_2O_3 films grown on 4H-SiC (0001) substrates. Note that the increment of the c_{RT}/a_{RT} ratio is probably attributed to the small domain size of the films grown on low T_g [14] from an analogy to a previous report on Ti_2O_3 nanoparticles [38] (also see Supplemental Material [23]). The minimum c_{RT}/a_{RT} ratio was 2.672 at a T_g of 1000°C, which was slightly larger than the c_{RT}/a_{RT} ratio of bulk Ti_2O_3 (c_{RT}/a_{RT} = 2.639, where a = 5.157 Å and c = 13.61 Å) [5]. The maximum

c_{RT}/a_{RT} ratio of 2.821 was observed at the lowest T_g (500℃). This c_{RT}/a_{RT} ratio was much larger than that of bulk Ti_2O_3 and comparable to that of V_2O_3 (c_{RT}/a_{RT} = 2.828, where a = 4.9717 Å and c = 14.005 Å) [39]. Consequently, the c_{RT}/a_{RT} ratio was controllable in the range of 2.672–2.821 owing to the similarity in the local structures of Ti_2O_3 and 4H-SiC on the (0001) planes.

Having confirmed that the c_{RT}/a_{RT} ratio of the Ti_2O_3 films was systematically controlled by varying T_g, we next investigated the transport properties of the Ti_2O_3 films. Figure 3 shows the temperature dependence of the resistivity (ρ–T curves) of the Ti_2O_3 films grown at various T_g, namely, with different c_{RT}/a_{RT} ratios. With decreasing T_g (increasing c_{RT}/a_{RT} ratio), a significant suppression of the MIT is clearly observed. For the Ti_2O_3 film grown at 1050℃, the ρ–T curve showed a significant drop in resistivity, starting at approximately 350 K and dropping by an order of magnitude over a wide temperature range of approximately 150 K. This is similar to the MIT behavior in bulk Ti_2O_3 [1–4, 7, 9, 10]. Therefore, it is logical to define the resistivity change as the characteristic MIT of Ti_2O_3 although the observed temperature was much lower (by approximately 100 K) than the T_{MIT} of bulk Ti_2O_3 (~450 K). As T_g decreased, the T_{MIT}

became lower with a smaller resistivity change and eventually decreased to ~150 K for the films grown at 700℃. Meanwhile, for the films grown below 700℃, a clear MIT was not observed; the ρ–T curves of the films were almost flat over the entire measured temperature range.

One might suspect that the lowering of T_{MIT} and disappearance of the MIT are due to extrinsic effects, such as oxygen non-stoichiometry at different T_g. However, this is unlikely to be the case for Ti_2O_3 for the following two reasons. First, the corundum-type Ti_2O_3 phase is known to be unstable to oxygen non-stoichiometry, and less than 1% oxygen non-stoichiometry compared to Ti atoms is tolerated in Ti_2O_3 [40]. Second, even if the introduced excess oxygen in Ti_2O_3 became an acceptor, the small number of hole carriers would hardly affect T_{MIT}, which has been demonstrated by the previous results for bulk $(Ti_{1-x}V_x)_2O_3$ [4, 5, 10]; T_{MIT} of $(Ti_{1-x}V_x)_2O_3$ remains almost unchanged (approximately 450 K) irrespective of substitutional V doping, which acts as excess oxygen, although the resistivity in low-temperature insulating phases is strongly suppressed [4, 10]. Therefore, the lowering of T_{MIT} and resultant disappearance of the

MIT observed from the ρ–T curves for the Ti_2O_3 films were attributed to the change in the c/a ratios.

In the ρ–T curves shown in Fig. 3, there are two characteristic temperatures. One is the above-mentioned T_{MIT}, which is defined as the temperature at which resistivity changes, similar to a step function. The other is the metallic conductivity temperature (T_{MC}), at which the ρ–T curve shows an upturn due to the metallic conductivity at high temperatures. To qualitatively discuss the change in the electronic phases of Ti_2O_3, T_{MIT} and T_{MC} were determined by the local minimum and zero points of the first derivative of the ρ–T curves ($d\rho/dT$), respectively (see Fig. S5 in Supplemental Material [23]). The values are plotted in Fig. 4(a) as functions of the corresponding c_{RT}/a_{RT} ratios. It should be noted that the determined T_{MIT} of 433 K for bulk Ti_2O_3 (Fig. 3) is in good agreement with the T_{MIT} of approximately 450 K [1–10], thereby confirming the validity of the analytical procedures.

A very close relationship between the T_{MIT} and c_{RT}/a_{RT} ratio is shown in Fig. 4(a). As the c_{RT}/a_{RT} ratio decreased to 2.75, the T_{MIT} of the Ti_2O_3 films linearly decreased with a slope of -3×10^3 K/(c/a). Surprisingly, the bulk data (T_{MIT} = 433 K,

c_{RT}/a_{RT} = 2.639) followed this extrapolated straight line, suggesting that the MIT in Ti_2O_3 was mainly dominated by the c/a ratio. In addition, the c_{RT}/a_{RT} ratio at T_{MIT} = 0 K was estimated to be 2.77, which is consistent with the experimental result in Fig. 3, where the MIT behavior disappears (T_{MIT} could not be determined from the ρ–T curves) for the films grown at 650, 600, and 500°C (with c_{RT}/a_{RT} ratios of 2.77, 2.79, and 2.82, respectively). The previous results for Ti_2O_3 films are also on the straight line [14], suggesting the universality of the relationship between the T_{MIT} and c/a ratio in Ti_2O_3.

The T_{MC} for $c_{RT}/a_{RT} \leq 2.77$ also had a similar linear relationship with almost the same slope of -3×10^3 K/(c/a). The coincidence between the T_{MIT} and T_{MC} behaviors suggests that the T_{MC} for $c_{RT}/a_{RT} \leq 2.77$ reflects an identical phenomenon to the T_{MIT}; the T_{MC} may not be the temperature of another transition but the onset temperature of the broad MIT in Ti_2O_3. In contrast to the behavior of T_{MIT}, T_{MC} deviated from the trend for $c_{RT}/a_{RT} \geq 2.77$. Because the MIT is absent for films with $c_{RT}/a_{RT} \geq$ 2.77 (for relatively low T_g values of 650, 600, and 500°C), the deviation may originate from extrinsic effects such as localization and/or scattering of conductive carriers at defects due to the poor crystallinity of the films grown at low T_g [41, 42].

Because the crystal deformation in Ti_2O_3 is also influenced by temperature, the effect of thermal lattice expansion should be considered for the phase transition phenomena occurring at different temperatures. Assuming that the Ti_2O_3 films show the same thermal lattice expansion as the bulk, we replotted the T_{MIT} and T_{MC} in Fig. 4(b) as a function of the *c*/*a* ratios that were calibrated using a thermal-expansion coefficient of 3.3×10^{-4} (*c*/*a*)/K for bulk Ti_2O_3 (see Fig. S6 in Supplemental Material [23]) [5, 6]. It is clear from the plot that the MIT in Ti_2O_3 occurs at a *c*/*a* ratio of 2.68 because the coefficient is nearly orthogonal to the slope of T_{MIT} vs. c_{RT}/a_{RT} ratio [-3×10^3 K/(*c*/*a*)]. These results indicate that the MIT phenomena in Ti_2O_3 are governed mainly by a critical *c*/*a* ratio of 2.68. Therefore, the temperature-induced insulator-to-metal transition in Ti_2O_3 occurs when the *c*/*a* ratio exceeds this critical value, owing to the thermal expansion of its crystal lattice.

DFT calculations also supported the modulation of the electric properties by the *c*/*a* ratio of Ti_2O_3. Figure 5(a) shows the calculated energy gap of Ti_2O_3 with various *c*/*a* ratios in the range of 2.639 to 2.82 (corresponding to the c_{RT}/a_{RT} ratios from the bulk to the film grown at 500℃). In the DFT calculation, the on-site Coulomb interaction

parameter U was set to 2.2 eV to reproduce the insulating phase of bulk Ti_2O_3, which has an energy gap of approximately 100 meV at a c/a ratio of 2.639 [5]. As shown in Fig. 5(a), an energy gap was formed at c/a = 2.639 and its size systematically decreased with increasing c/a ratio. At c/a = 2.68, the energy gap is closed, indicating that this is a critical c/a ratio. Subsequently, the metallic states remain stable for $c/a \leq 2.82$. These results indicate the occurrence of lattice-deformation-driven MIT in Ti_2O_3 at a critical c/a ratio. Furthermore, the excellent agreement of the critical c/a ratio between the experiments and calculations suggests the validity of the present DFT + U calculation for describing the electronic structure of Ti_2O_3.

To observe the change in electronic structures across the MIT in more detail, the typical DOS near E_F of insulating Ti_2O_3 (c/a = 2.66) and metallic Ti_2O_3 (c/a = 2.70) are shown in Figs. 5(b) and (c), respectively. The overall DOS shapes were similar for the insulating and metallic Ti_2O_3. However, a closer inspection of E_F revealed that the small energy gap formed in the insulating Ti_2O_3 was closed by the slight overlap of the Ti 3d states below and above E_F in metallic Ti_2O_3, which is schematically shown in the inset of Fig. 5(a). These results demonstrate that the MIT is not a Mott transition

induced by temperature but a gradual semimetal-to-semiconductor transition induced by lattice deformation.

The present study provides clear evidence that the MIT of Ti_2O_3 originates from lattice deformation, although it should be noted that the present study does not rule out the importance of dynamic electronic interactions for the MIT in Ti_2O_3 [16]. We used epitaxial films to investigate the relationship between the MIT and *c*/*a* ratio. An alternative approach is the temperature- and pressure-dependent investigation of the structural and electronic properties of a single bulk specimen under high uniaxial pressure. Such a high-pressure study of bulk materials would more precisely reveal the essential correlation of the MIT with the Ti–Ti distances instead of the *c*/*a* ratio. The detailed structural parameters for the Ti–Ti distances along the *c*-axis and in the *a*–*b* plane, which are directly correlated to the a_{1g} and e_g^{π} bands**,** would provide useful information on the contribution of dynamic electronic interactions to the MIT and pave the way for more realistic calculations incorporating intersite electron correlations.

CONCLUSION

In conclusion, we synthesized corundum-type Ti_2O_3 films on 4H-SiC (0001) substrates and investigated their structural and electronic properties. Films with wide c_{RT}/a_{RT} ratios ranging from 2.672 to 2.821 were achieved in a controllable fashion by changing T_g. MIT was observed for films with $c_{RT}/a_{RT} \leq 2.75$, whereas MIT was absent for those with $c_{RT}/a_{RT} \geq 2.77$. We found that the T_{MIT} was proportional to the c_{RT}/a_{RT} ratio, and the MIT occurred at a critical value of 2.68 in both the Ti_2O_3 bulk and films. Systematic DFT + U calculations with reasonable parameters confirmed that the MIT occurred at a critical c/a ratio of 2.68. The good agreement between the experimental and simulated MIT behaviors based on the c/a ratio indicated that the MIT is not a Mott transition induced by temperature, but a gradual semimetal-to-semiconductor transition induced by lattice deformation.

ACKNOWLEDGEMENTS

We thank R. Kumashiro and K. Saitoh in the common equipment room of Advanced Institute for Materials Research at Tohoku University for their assistance

with Raman spectroscopy, XRD, and film-thickness measurements. This work was partly supported by the MEXT Elements Strategy Initiative to Form Core Research Center (JPMXP0112101001), Grant-in-Aid for Scientific Research (Nos. 22H01947 and 22H01948) from the Japan Society for the Promotion of Science Foundation, CREST (JPMJCR18T1) from the Japan Science and Technology Agency (JST), Asahi Glass Foundation, Nagamori Foundation, Research Foundation for the Electrotechnology of Chubu, Toyota Riken Scholar Program, and Iketani Science and Technology Foundation. N.H. acknowledges the financial support from the Chemistry Personnel Cultivation Program of the Japan Chemical Industry Association. The authors would also like to thank Editage for English language editing.

277 **REFERENCES**

278 [1] F. J. Morin, Phys. Rev. Lett. **3**, 34 (1959). DOI: 10.1103/PhysRevLett.3.34.

279 [2] J. M. Honig, Rev. Mod. Phys. **40**, 748 (1968). DOI: 10.1103/RevModPhys.40.748.

280 [3] J. M. Honig and T. B. Reed, Phys. Rev. **174**, 1020 (1968). DOI:

281 10.1103/PhysRev.174.1020.

282 [4] M. Uchida, J. Fujioka, Y. Onose, and Y. Tokura, Phys. Rev. Lett. **101**, 066406 (2008).

283 DOI: 10.1103/PhysRevLett.101.066406.

284 [5] J. J. Capponi, M. Marezio, J. Dumas, and C. Schlenker, Solid State Commun. **20**,

285 893 (1976). DOI: 10.1016/0038-1098(76)91299-0.

286 [6] C. N. R. Rao, R. E. Loehman, and J. M. Honig, Phys. Lett. **27A**, 271 (1968). DOI:

287 10.1016/0375-9601(68)90696-8.

288 [7] L. L. Van Zandt, J. M. Honig, and J. B. Goodenough, J. Appl. Phys. **39**, 594 (1968).

289 DOI: 10.1063/1.2163536.

290 [8] H. J. Zeiger, Phys. Rev. B **11**, 5132 (1975). DOI: 10.1103/PhysRevB.11.5132.

291 [9] C. F. Chang, T. C. Koethe, Z. Hu, J. Weinen, S. Agrestini, L. Zhao, J. Gegner, H. Ott,

292 G. Panaccione, H. Wu, M. W. Haverkort, H. Roth, A. C. Komarek, F. Offi, G. Monaco,

293 Y. -F. Liao, K. -D. Tsuei, H. -J. Lin, C. T. Chen, A. Tanaka, and L. H. Tjeng, Phys. Rev.

294 X **8**, 021004 (2018). DOI: 10.1103/PhysRevX.8.021004.

295 [10] G. V. Chandrashekhar, Q. Won Choi, J. Moyo, and J. M. Honig, Mat. Res. Bull. **5**,

296 999 (1970). DOI: 10.1016/0025-5408(70)90048-6.

297 [11] L. F. Mattheiss, J. Phys.: Condens. Mater **8**, 5987 (1996). DOI:

298 10.1088/0953-8984/8/33/007.

299 [12] Y. Guo, S. J. Clark, and J. Robertson, J. Phys.: Condens. Mater **24**, 325504 (2012).

300 DOI: 10.1088/0953-8984/24/32/325504.

301 [13] K. Yoshimatsu, H. Kurokawa, K. Horiba, H. Kumigashira, and A. Ohtomo, APL

302 Mater. **6**, 101101 (2018). DOI: 10.1063/1.5050823.

303 [14] K. Yoshimatsu, N. Hasegawa, Y. Nambu, Y. Ishii, Y. Wakabayashi, and H.

304 Kumigashira, Sci. Rep. **10**, 22109 (2020). DOI: 10.1038/s41598-020-79182-5.

305 [15] N. Hasegawa, K. Yoshimatsu, D. Shiga, T. Kanda, S. Miyazaki, M. Kitamura, K.

306 Horiba, and H. Kumigashira, "Electronic band structure of Ti_2O_3 thin films studied by

307 angle-resolved photoemission spectroscopy" Phys. Rev. B **105**, 235137 (2022). DOI:

308 10.1103/PhysRevB.105.235137.

309 [16] A. I. Poteryaev, A. I. Lichtenstein, and G. Kotliar, Phys. Rev. Lett. **93**, 086401
310 (2004). DOI: 10.1103/PhysRevLett.93.086401.
311 [17] Y. Li, Y. Weng, J. Zhang, J. Ding, Y. Zhu, Q. Wang, Y. Yang, Y. Cheng, Q. Zhang,
312 P. Li, J. Lin, W. Chen, Y. Han, X. Zhang, L. Chen, X. Chen, J. Chen, S. Dong, X. Chen,
313 and T. Wu, NPG Asia Mater **10**, 522 (2018). DOI: 10.1038/s41427-018-0050-5.
314 [18] P. V. Shvets, D. Caffrey, K. Fleischer, I. Shvets, K. O'Neill, G. S. Duesberg, A. N.
315 Vinichenko, K. Y. Maksimova, and A. Y. Goikhman, Thin Solid Films **694**, 137642
316 (2020). DOI: 10.1016/j.tsf.2019.137642.
317 [19] C. Zhang, F. Hao, G. Gao, X. Liu, C. Ma, Y. Lin, Y. Lin, and X. Li, NPJ Quantum
318 Mater. **2**, 2 (2017). DOI: 10.1038/s41535-016-0006-3.
319 [20] K. Yoshimatsu, O. Sakata, and A. Ohtomo, Sci. Rep. **7**, 12544 (2017). DOI:
320 10.1038/s41598-017-12815-4.
321 [21] J. B. Casady and R. W. Johnson, Solid-State Electron. **39**, 1409 (1996). DOI:
322 10.1016/0038-1101(96)00045-7.
323 [22] K. Momma and F. Izumi, J. Appl. Cryst. **44**, 1272 (2011). DOI:
324 10.1107/S0021889811038970.
325 [23] See Supplemental Material at

326 http://link.aps.org/supplemental/XXXXXXXXXXXXX for schematic surface structures
327 of 4H-SiC and Ti_2O_3; out-of-plane XRD patterns, Raman spectra, XRD φ-scan, and first
328 derivative of the resistivity curves of the films; and temperature dependence of the *c*/*a*
329 ratios for bulk Ti_2O_3.
330 [24] K. Yoshimatsu and H. Kumigashira, Cryst. Growth Des. **22**, 703 (2022). DOI:
331 10.1021/acs.cgd.1c01214.
332 [25] H. Kurokawa, K. Yoshimatsu, O. Sakata, and A. Ohtomo, J. Appl. Phys. **122**,
333 055302 (2017). DOI: 10.1063/1.4997443.
334 [26] A. Mooradian and P. M. Raccah, Phys. Rev. B **3**, 4253 (1971). DOI:
335 10.1103/PhysRevB.3.4253.
336 [27] S. H. Shin, R. L. Aggarwal, B. Lax, and J. M. Honig, Phys. Rev. B **9**, 583 (1974).
337 DOI: 10.1103/PhysRevB.9.583.
338 [28] S. H. Shin, F. H. Pollak, T. Halpern, and P. M. Raccah, Solid State Commun. **16**,
339 687 (1975). DOI: 10.1016/0038-1098(75)90453-6.
340 [29] S. P. S. Porto and R. S. Krishnan, J. Chem. Phys. **47**, 1009 (1967). DOI:
341 10.1063/1.1711980.

342 [30] X. Li, A. L. Zhu, W. Qu, H. Wang, R. Hui, L. Zhang, and J. Zhang, Electrochim.
343 Acta **55**, 5891 (2010). DOI: 10.1016/j.electacta.2010.05.041.
344 [31] Y. Wu, Q. Zhang, X. Wu, S. Qin, and J. Liu, J. Solid State Chem. **192**, 356 (2012).
345 DOI: 10.1016/j.jssc.2012.04.036.
346 [32] A. Ould-Hamouda, H. Tokoro, S.-I. Ohkoshi, and E. Freysz, Chem. Phys. Lett. **608**,
347 106 (2014). DOI: 10.1016/j.cplett.2014.05.073.
348 [33] P. Giannozzi, S. Baroni, N. Bonini, M. Calandra, R. Car, C. Cavazzoni, D. Ceresoli,
349 G. L. Chiarotti, M. Cococcioni, I. Dabo, *et al*., J. Phys.: Condens. Matter **21**, 395502
350 (2009). DOI: 10.1088/0953-8984/21/39/395502.
351 [34] P. Giannozzi, O. Andreussi, T. Brumme, O. Bunau, M. B. Nardelli, M. Calandra, R.
352 Car, C. Cavazzoni, D. Ceresoli, M. Cococcioni, *et al*., J. Phys.: Condens. Matter **29**,
353 465901 (2017). DOI: 10.1088/1361-648X/aa8f79.
354 [35] J. P. Perdew, K. Burke, and M. Ernzerhof, Phys. Rev. Lett. **77**, 3865 (1996). DOI:
355 10.1103/PhysRevLett.77.3865.
356 [36] H. J. Monkhorst and J. D. Pack, Phys. Rev. B **13**, 5188 (1976). DOI:
357 10.1103/PhysRevB.13.5188.

358 [37] P. E. Blöchl, O. Jepsen, and O. K. Andersen, Phys. Rev. B **49**, 16223 (1994). DOI:
359 10.1103/PhysRevB.49.16223.
360 [38] S. Tsujimoto, Y. Matsushita, S. Yu, K. Yamaura, and T. Uchikoshi, J. Asian Ceram.
361 Soc. **3**, 325 (2015). DOI: 10.1016/j.jascer.2015.06.007
362 [39] D. B. McWhan, T. M. Rice, and J. P. Remeika, Phys. Rev. Lett. **23,** 1384 (1969).
363 DOI: 10.1103/PhysRevLett.23.1384.
364 [40] S. Andersson, B. Collén, U. Kuylenstierna, and A. Magnéli, Acta Chem. Scand. **11**,
365 1641 (1957). DOI: 10.3891/acta.chem.scand.11-1641.
366 [41] P. W. Anderson, Phys. Rev. **109**, 1492 (1958). DOI: 10.1103/PhysRev.109.1492.
367 [42] A. Möbius, Crit. Rev. Solid State Mater. Sci. **44**, 1 (2019). DOI:
368 10.1080/10408436.2017.1370575.

FIGURES

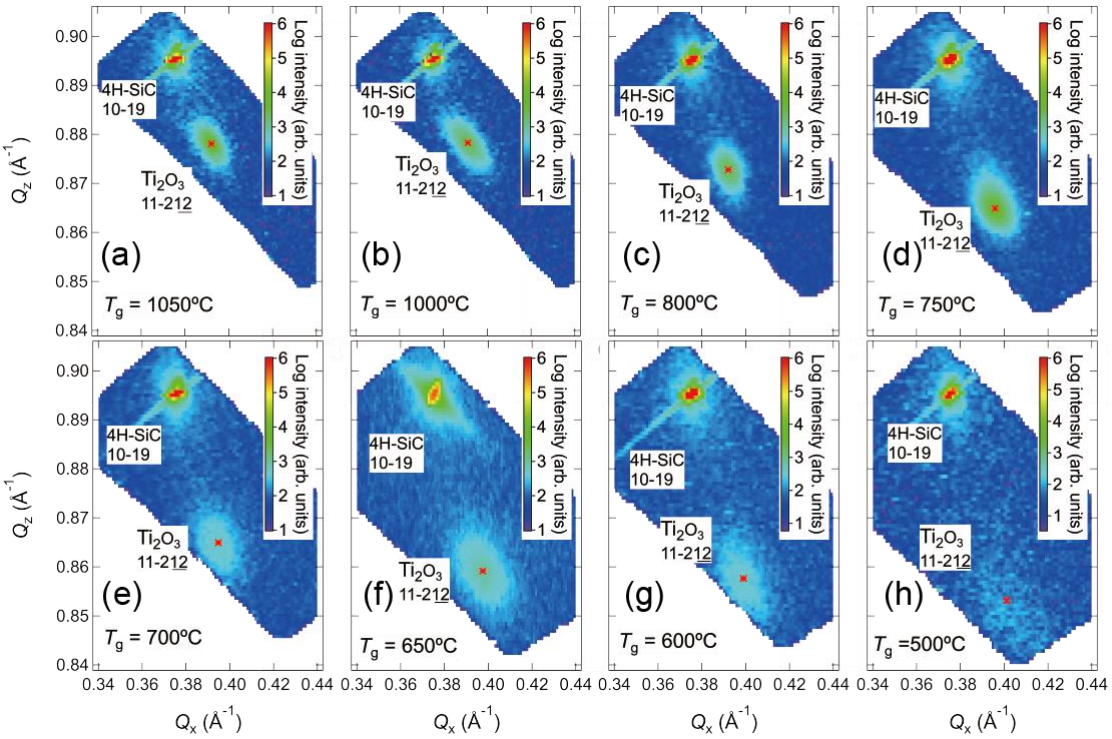


Figure 1. Yoshimatsu *et al*.

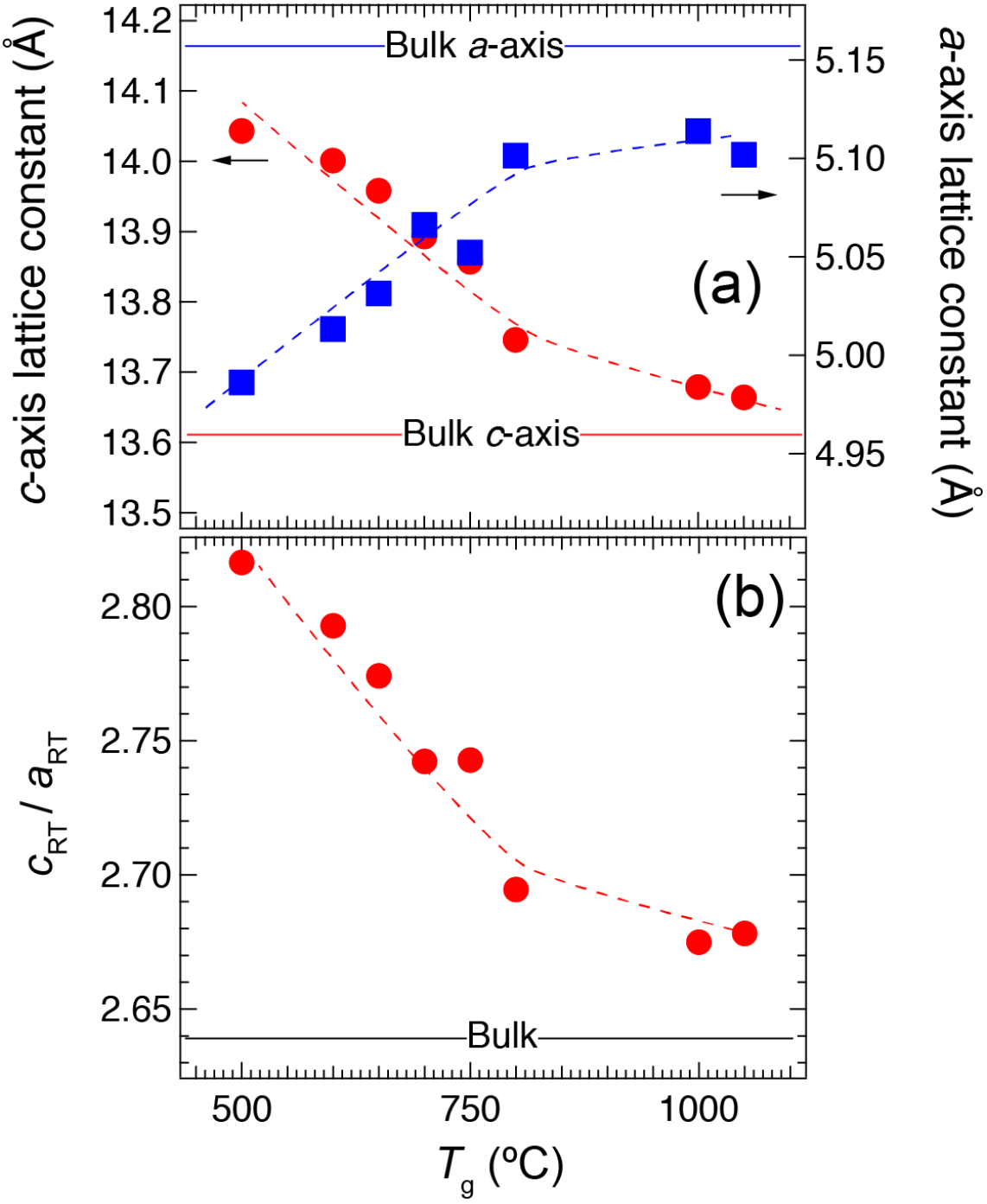


Figure 2. K. Yoshimatsu *et al*.

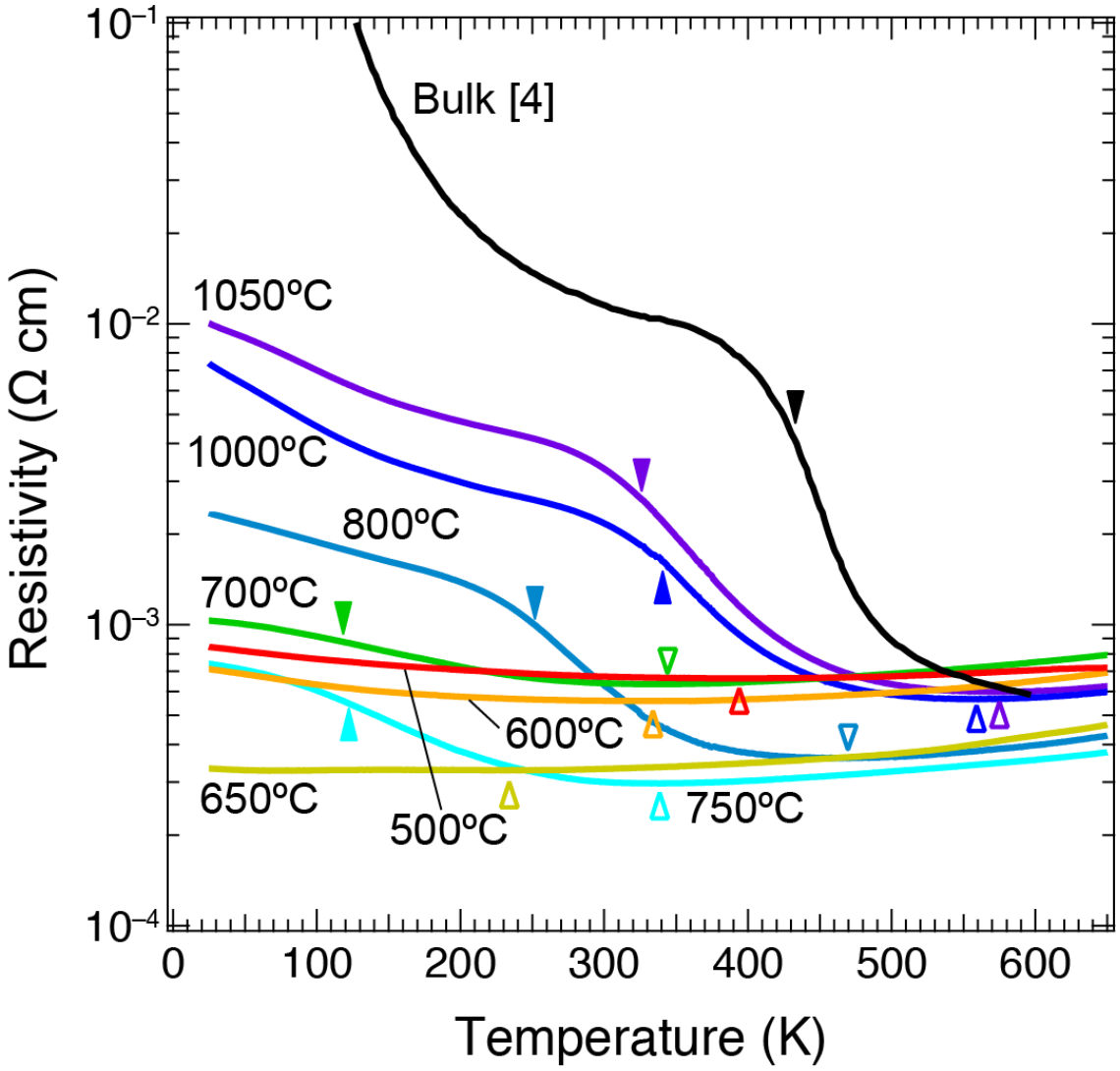


Figure 3. K. Yoshimatsu *et al*.

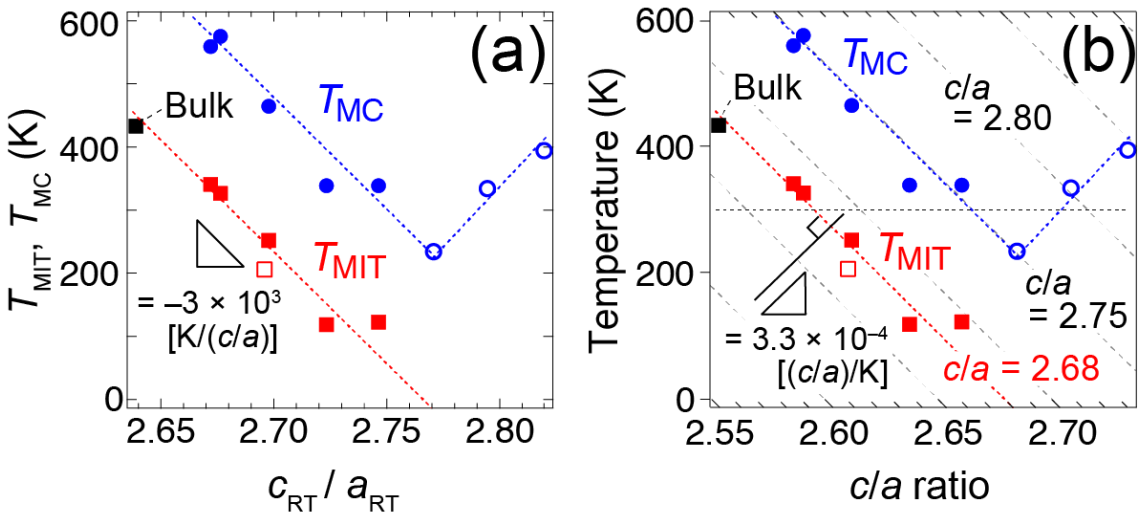
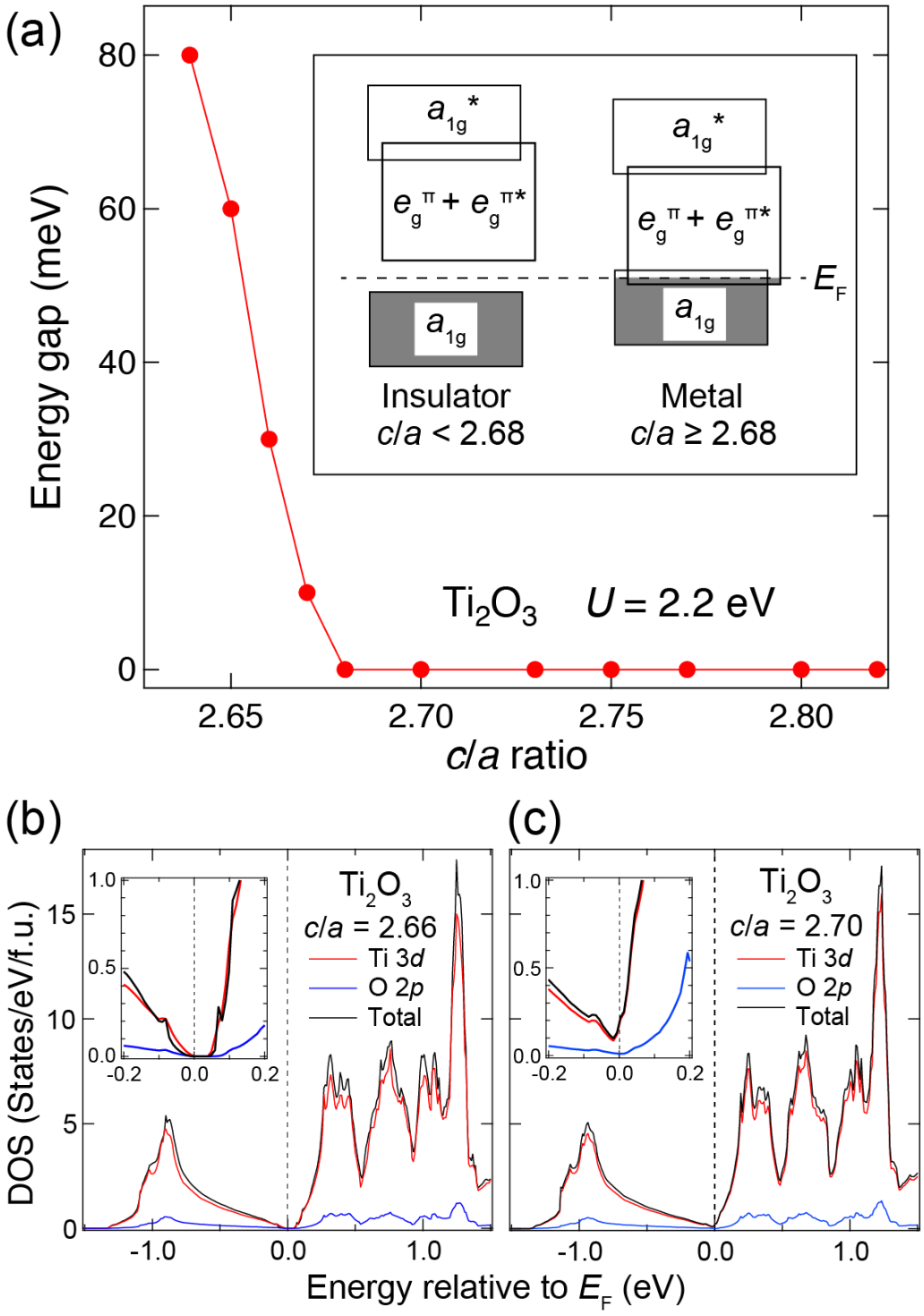


Figure 4. K. Yoshimatsu *et al*.



401

402 Figure 5. K. Yoshimatsu *et al*.

403

FIGURE CAPTIONS

FIG. 1

Reciprocal space maps around 4H-SiC 10–19 reciprocal points for Ti_2O_3 films grown at (a) 1050°C, (b) 1000°C, (c) 800°C, (d) 750°C, (e) 700°C, (f) 650°C, (g) 600°C, and (h) 500°C. Ti_2O_3 11–2$\underline{12}$ reciprocal points are indicated by the red markers.

FIG. 2

(a) *a*-axis and *c*-axis lattice constants and (b) *c*/*a* ratios at RT (c_{RT}/a_{RT}) of the Ti_2O_3 films prepared at growth temperatures (T_g) of 500–1050°C. Solid lines indicate the values for bulk Ti_2O_3 [5, 6]. The dashed lines are guides to the eye.

FIG. 3

Temperature dependence of resistivity (ρ–T curve) for the Ti_2O_3 films grown at temperatures of 500–1050°C. The ρ–T curve for bulk Ti_2O_3 is also shown as a reference [4]. Filled and open triangles indicate T_{MIT} and T_{MC} that were determined from the first derivative of the ρ–T curves, respectively. (See Fig. S5 in Supplemental Material [23]).

FIG. 4

(a) Plots of T_{MIT} and T_{MC} as a function of c_{RT}/a_{RT}. The dashed lines are guides for the eye. (b) Plots of T_{MIT} and T_{MC} as a function of the c/a ratios that were calibrated by the temperature-induced lattice deformation. (See Fig. S6 in Supplemental Material [23]). Dotted diagonal lines indicate the coordinate for the same c/a ratio. Red open squares indicate the data of the Ti_2O_3 film grown on α-Al_2O_3 (0001) substrates (c_{RT}/a_{RT} = 2.696 and T_{MIT} = 206 K) [14]. Blue open circles indicate T_{MC} of the films in which the MIT is absent.

FIG. 5

(a) Energy gap at the Fermi level (E_F) as a function of the c/a ratios. The energy gap was obtained from DFT calculations with U = 2.2 eV [11, 14, 15]. The inset shows schematic band diagrams of insulating and metallic Ti_2O_3 near E_F. Calculated densities of states near E_F with c/a ratios of (b) 2.66 and (c) 2.70. Insets of (b) and (c) show the corresponding magnifications near E_F.